



PLANETARY SCIENCE

Saturn's F ring is intermittently shepherded by Prometheus

Jeffrey N. Cuzzi^{1*}, Essam A. Marouf², Richard G. French³, Carl D. Murray⁴, Nicholas J. Cooper⁴

One of the stranger planetary rings is Saturn's narrow, clumpy F ring, lying just outside the main rings, in a region disturbed by chaotic orbital dynamics. We show that the F ring has a stable "true core" that dominates its mass and is confined into discontinuous short arcs of particles larger than a few millimeters in radius. The more obvious micron-size particles seen in images, outlining and obscuring the true core, contribute only a small fraction of its mass. We found that these arcs of large particles orbit Saturn in a specific corotational resonance with the nearby 100-kilometer diameter ringmoon Prometheus, which stabilizes the F ring material and allows it to persist within the disturbed region for decades or longer. Toward the end of the observing period, a small chaotic glitch in the orbit of Prometheus temporarily disrupted the confinement, but the arcs seem to be able to adapt.

INTRODUCTION

The first images of Saturn's F ring, from Voyager 1, were puzzling to dynamicists and captivating to everyone (1). The ring appeared to be an ensemble of closely spaced narrow strands, which showed odd kinks and even appeared to be braided or overlapping. Since that time, Cassini has both advanced our understanding and nourished our puzzlement (2). The material seen in F ring images and stellar occultations is dominated by tiny, micron-sized grains, that must be constantly resupplied from more massive but unseen particles (3). More evidence for large particles has come from a small spread in orbital radius of transient clumps (4–6) and so-called "mini-jets" (7) caused by gentle collisions within the ring.

The persistence of Voyager's F ring was quickly ascribed to a then-new "shepherding" process by which moonlets straddling a narrow ring could confine the ring by balancing oppositely directed torques (8) and in some way could cause the kinks as well. However, concern soon arose that the slightly more massive inner moonlet Prometheus was closer to the ring than its supposed outer companion "shepherd" Pandora, calling the balance of torques idea into question (9). The situation became even more puzzling when it was realized that the entire F ring region was dynamically chaotic; that is, perturbations by Prometheus cause any particle in the region to undergo substantial, and unpredictable, orbital changes on time scales of weeks or months (10–12). There is evidence for just such chaotic motions in rare objects crossing the F ring (13), and yet the F ring itself has persisted from the Voyager Saturn encounters in 1980–1981 to today in basically the same orbit (14).

A partial solution was suggested by Cuzzi *et al.* (15) who found narrow, dynamically stable zones in numerical simulations, very close to predicted locations for first-order outer Lindblad resonances (LRs), one of which coincided within uncertainty with the F ring. Realizing that these resonances were more likely to disperse than to stabilize ring material, they speculated on different possibilities for ring stabilization. Most of the discussion centered on new physics they called an "antiresonance," but they also speculated that corotation resonances (CRs) might be responsible [as had been suggested for Neptune's Adams ring; (16, 17)]. Subsequently, an error was found

in the antiresonance formulation (18), and we will not discuss it further here.

Here, we present Cassini Radio Science (RSS) observations showing that the F ring's mass is dominated by a "true core" locally <1 km in radial width, made of particles larger than a few millimeters, that is structured as a chain of disconnected "arcs" in the same orbit. We show that the arcs are restricted to longitudes controlled by the $m = 110$ corotation-eccentricity resonance (CER) with Prometheus, allowing the most problematic encounter geometries with Prometheus to be avoided (see section S3).

RESULTS

The Cassini Radio Science Subsystem (RSS) Team has, since the beginning of the mission, observed numerous occultations of the spacecraft radio signals at 0.94-, 3.6-, and 13-cm wavelength by Saturn's rings, in various geometries. The original diffraction-limited measurements were reconstructed to resolve radial features as narrow as a few hundred meters. In 66 ingress or egress occultations between May 2005 and August 2013, the F ring was unambiguously detectable in only 23 RSS occultations or about 35% of the time, and when seen (in many cases), it was seen at all three wavelengths (section S2 and tables S1 to S4). The detections almost always reveal a single strand, a few hundred meters to about 1-km wide, and of (wavelength-dependent) peak normal optical depth (eq. S1) of a few to several tenths with some exceptions. RSS senses diffraction by ring structure, which is azimuthally extended over more than a Fresnel scale (few to several km), that is, assemblages of particles collectively acting as a one-dimensional, partially transparent, diffraction screen (19). Because radio signals primarily sense particles of radius comparable to the wavelength or larger, a distribution of particles with radius larger than a few millimeters, and even as large as several centimeters (when the 13-cm wavelength signal is affected), appears to dominate the true core surface mass density (section S7). The generally visible F ring micron-size dust covering all longitudes, which delineates the strands of 10- to 30-km radial width that are routinely seen in images and stellar occultations (20), is transparent to these longer-wavelength occultations.

We consider whether these sporadic detections manifest longitudinal dynamical confinement of material, such as the arcs in Neptune's Adams ring. The narrow stable zones of (15) were all close to first-order LR with Prometheus (section S3). LR excite eccentricity and

¹Ames Research Center, NASA, Moffett Field CA 94035, USA. ²San Jose State University, San Jose, CA, USA. ³Wellesley College, Wellesley, MA, USA. ⁴Queen Mary University of London, London, UK.

*Corresponding author. Email: jeffrey.cuzzi@nasa.gov

Copyright © 2024 the Authors, some rights reserved; exclusive licensee American Association for the Advancement of Science. No claim to original U.S. Government Works. Distributed under a Creative Commons Attribution NonCommercial License 4.0 (CC BY-NC).

are usually perturbed locations, not stable ones (21). Meanwhile, each first-order LR is also accompanied by a small family of traditional resonances of slightly different kinds (see section S3 and fig. S3), and different theories of the Neptune arc confinement have relied on various combinations of these. In the F ring case, the resonance optimally capable of stabilizing the ring material is a CER (21) because in such a resonance, orbital conjunctions between Prometheus and specific F ring longitudes are phased to occur only when Prometheus is at its periapse, furthest from the F ring and least likely to deliver a strong enough gravitational impulse to send the ring particles off onto chaotically diverging orbits (15). Moreover, the best previous estimates of the F ring’s semimajor axis implied that the CER of interest would have to be the $m = 110$ CER (fig. S3). Because the gravitational potential of an m -th order resonance has m lobes (section S3), F ring material orbiting in the $m = 110$ CER should have 110 lobes or arcs, each of angular width about 3.3° . This provides a test of the CER hypothesis.

To test the hypothesis, we started with the times and longitudes of RSS occultation detections and nondetections (the latter obtained from predictions of a mean F ring orbit model). We regressed the longitudes of the 23 Cassini detections, the single Voyager detection, and all 43 Cassini nondetections to a common reference time t^* using the mean motions (n) given by a range of $m = 110$ CER pattern speeds, each in turn associated with one of a “comb” of finely gridded

candidate Prometheus mean motions (n_{Pr} ; see eq. S14). The periapse longitude of Prometheus was also regressed to t^* (see section S1 for details). The longitude differences between each arc and Prometheus periapse (all at t^*), which span 360° of orbit longitude, were then folded modulo $m=110$, as if all the separations from Prometheus periapse were combined into one cycle of $360^\circ/m = 3.27^\circ$. Clustering around zero in this folded coordinate would confirm the hypothesis that the specified CR localizes stable F ring material into favored longitudes that encounter Prometheus only when it is near its periapse (i.e., when unusually strong, chaos-inducing perturbations can be avoided).

The regression technique demands, and provides, a precision of about 10^{-6} because many of the arcs are regressed about 10^4 orbits into a lobe of angular width of about 0.01 orbits. To capture this precision, we used a range of constant values for candidate n_{Pr} , with fractional steps of 5×10^{-7} . Each n_{Pr} determined a new mean motion n_F for the $m=110$ CER (eq. S14) and a new regression/folding result. Only one fully credible solution for n_{Pr} was obtained, and it lay within two parts in a million of the two best prior independent determinations (see section S4 for more details).

Arc longitude clustering results for the single best solution for Prometheus’ n_{Pr} are shown in Fig. 1. Here, the horizontal axis range shows the regressed and folded arc longitudes in degrees, as measured

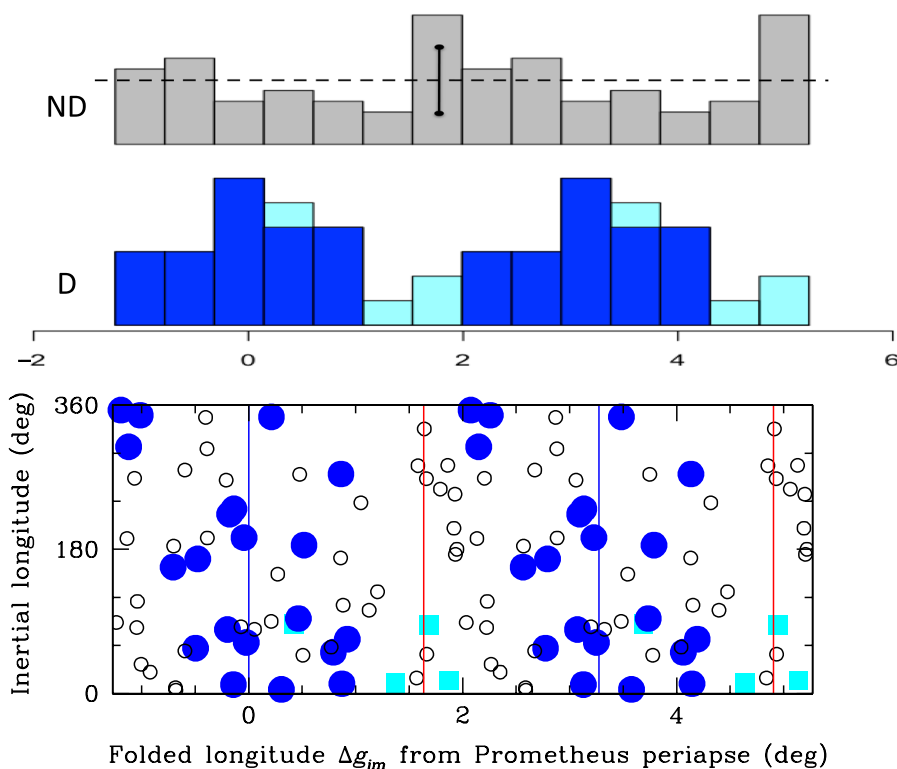


Fig. 1. Angular locations of F ring detections and nondetections. (Bottom) Filled symbols show Cassini RSS F ring detection longitudes, and open symbols show nondetection longitudes, all regressed to a common time, t^* (see section S4). The vertical axis shows the inertial orbital longitudes of the j detections g_{j}^* at t^* , covering 360° . The horizontal axis (denoted Δg_{jm} in section S1) is the folded (modulo $m = 110$) difference between each detection longitude and the longitude of Prometheus periapse at t^* . The plotted horizontal axis actually repeats two folded “cycles” of $\Delta g_{jm} = 0$, each of angular width $360^\circ/m = 3.27^\circ$, for visibility. The nondetections seem randomly distributed in both coordinates. The dark blue circles align preferentially with the (more stable) longitude of Prometheus’ periapse (blue vertical lines at $\Delta g_{jm} = 0$) and avoid the (less stable) longitude of its apoapse (red vertical lines one-half cycle away). The cyan squares—three lying near the “forbidden” red vertical lines—are the last four detections of the mission, which we argue should be ignored because they had been corrupted by a recent encounter with Prometheus on a recently altered orbit (section S4). **(Top)** We simply bin the detections (blue-cyan) and nondetections (gray) to better illustrate the clustering of the detections. The nondetection panel shows the mean and SD of the counts per bin. D, detection; ND, nondetection.

from the corresponding similarly regressed and folded periapse longitudes of Prometheus. One entire cycle of maximum and minimum stability covers $360^\circ/m = 3.27^\circ$ of orbit longitude, and the figure repeats the cycle twice for visibility. The most reliable detections (blue filled symbols) are all clustered within $\pm 1^\circ$ of the similarly regressed and folded longitudes of Prometheus' periapse (vertical blue lines), as predicted by the CER hypothesis. The red vertical lines 0.5 cycles away from regressed and folded periapses indicate unfavorable longitudes aligned with Prometheus apoapses.

The cyan points near the unfavorable longitudes show the last four arc detections in 2013 at the end of our observing period. The mean motion of Prometheus n_{Pr} is known to vary slightly with time due to Saturn system gravitational interactions and is also known to incur large, somewhat impulsive, jumps due to chaotic interactions with Pandora (22–24). Shortly before the Cassini RSS observational period began, Prometheus incurred a fractional change in n_{Pr} of about 5×10^{-6} , and we argue in the section S4 that it incurred a similar orbit change in early 2013, just before the last four RSS detections were obtained, corrupting them for the purpose of testing our hypothesis.

The $\pm 1^\circ$ scatter of the most credible (blue) stable arcs (roughly 70% of a cycle) may indicate libration about the most stable longitudes and/or manifest uncertainty in our Prometheus periapse values (section S3). Longitude uncertainty from the RSS detection timing approach is less than the width of the symbols (section S2). Using simple binomial statistics, we find that the probability of the observed clustering occurring by chance, into only about 70% of the available longitude space in each 3.27° cycle, is roughly 0.001 to 0.01, depending on whether we exclude or include those last four suspect detections (section S5).

We also conducted two additional independent validation tests on the hypothesis with results shown in Fig. 2. One test has somewhat of a brute-force nature, but the significance of it is easy to grasp. While Fig. 1 shows that the arc longitudes are consistent with Prometheus periapse longitudes, it does not prove that Prometheus was actually at periapse when it encountered the arcs. The top panel of Fig. 2, with details given in section S1, shows this directly, and statistics indicates that this prediction does seem to be satisfied. The second test (bottom panel of Fig. 2, with details given in section S2) is more elegant but more abstruse. We converted the arc detection longitudes

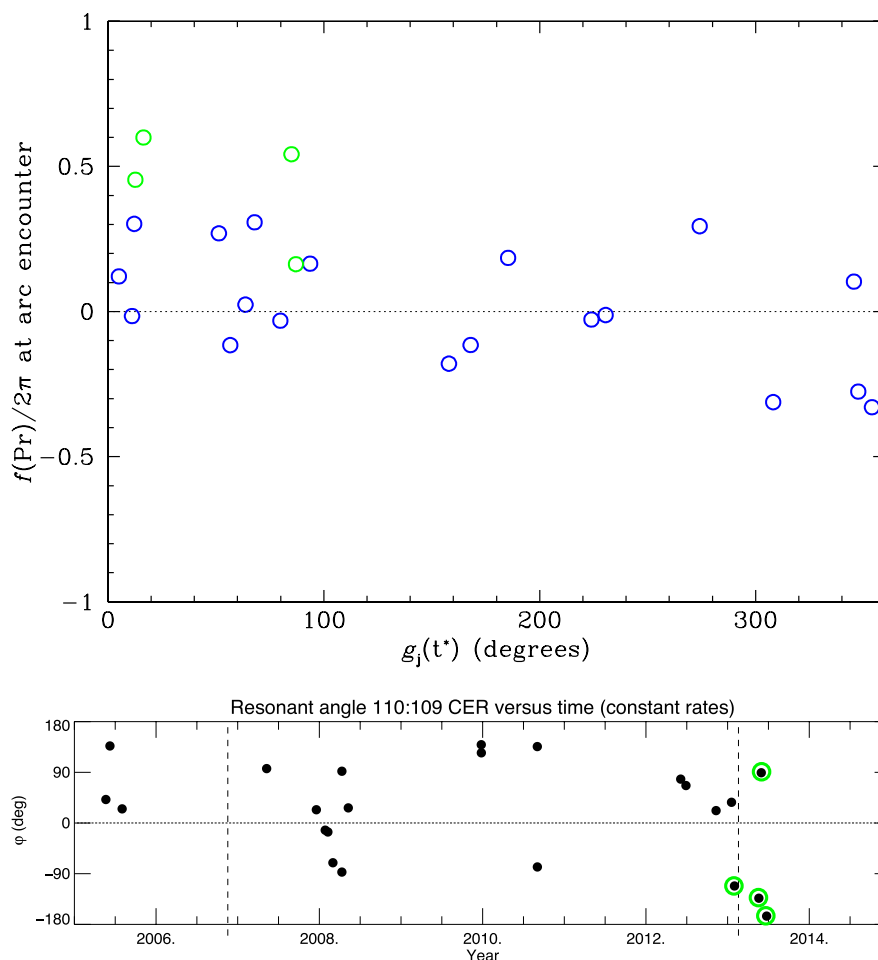


Fig. 2. Two additional tests of the CER hypothesis. (Top) A brute force test, in which the longitudes of the arcs and Prometheus (and the periapse of Prometheus) are integrated and the mean anomaly of Prometheus recorded when an encounter occurs with each arc. In the CER hypothesis, Prometheus should be at or near its periapse (mean anomaly = 0) when it encounters an arc, furthest from the arc and perturbing it only weakly. This seems to be consistent with the data, on average, although there seems to be a trend (unexplained) with inertial longitude. The final four arc detections of the mission are shown in green; we have argued that by this time, Prometheus had glitched to a new orbit, so their larger divergence is not problematic for the hypothesis. **(Bottom)** Resonance variable ϕ (eq. S19) for the arcs and Prometheus as a function of arc detection time. The final four arc detections of the mission are circled in green; as above, the large divergence of three of them is not problematic for the hypothesis.

to mean anomalies and constructed a resonance variable parameter using these and the contemporaneous Prometheus mean anomalies. In a true resonance such as the $m = 110$ CER we propose, the resonance variable should always be zero (21), and indeed, we find that (given the amount and plausible nature of the scatter as discussed above) this condition is probably satisfied.

DISCUSSION

Populated arcs may not cover all of available inertial longitude space; Fig. 1 hints at a depleted region between regressed inertial longitudes of $\sim 90^\circ$ to 150°). Since only one-third of all RSS occultations detect material, only about one-half of all dynamically stable lobes may be populated, consistent with many nondetections seen at stable longitudes relative to Prometheus periapse (open symbols in Fig. 1). Filled and empty lobes can lie near each other. We estimate from the angular extent, radial width, optical depth, and particle size properties of the RSS detections that the mass of the <1 -km wide true core of several millimeter (or larger) radius particles is at least 1000 times the mass of all the typically observed micron-sized dust strands (section S7).

There is a CER closely aligned with every LR in the F ring region, just as there were numerous narrow stable zones seen in the short-term numerical simulations of (15)—one near each LR. Moreover, Cuzzi *et al.* (15) show that all the numerically stable regions act like “attractors” or traps for chaotically diffusing particles even on short time scales. So one question remains now, what is unique about this particular CER and why is there only one F ring instead of stable material in many similar sites in the region.

During our period of analysis, we find that Prometheus’ mean motion was $n_{Pr} = 587.285415 \pm 0.00029$ degree/day, and the F ring true core semimajor axis (location of the $m = 110$ CER) was 140222.43 ± 0.05 km (table S1). Because Prometheus’ orbit does evolve chaotically by small increments (and we think we have seen one such event), the true core material must be able to adapt and track stable sites that move by small amounts now and then (see section S4). Perhaps an even more notable problem, which our theory does not resolve, is how these disconnected arcs manage to maintain a common, uniformly precessing, eccentric orbit (see section S7 for more discussion).

Supplementary Materials

This PDF file includes:

Supplementary Text
Figs. S1 to S7
Tables S1 to S5
Legend for movie S1
References

Other Supplementary Material for this manuscript includes the following:

Movie S1

REFERENCES AND NOTES

- B. A. Smith, L. Soderblom, R. Beebe, J. Boyce, G. Briggs, A. Bunker, S. A. Collins, C. J. Hansen, T. V. Johnson, J. L. Mitchell, R. J. Terrile, M. Carr, A. F. Cook II, J. Cuzzi, J. B. Pollack, G. E. Danielson, A. Ingersoll, M. E. Davies, G. E. Hunt, H. Masursky, E. Shoemaker, D. Morrison, T. Owen, C. Sagan, J. Veverka, R. Strom, V. E. Suomi, Encounter with Saturn - Voyager 1 imaging science results. *Science* **212**, 163–191 (1981).
- C. D. Murray, R. S. French, The F Ring of Saturn, in *Planetary Ring Systems, Properties, Structure, and Evolution*, M. S. Tiscareno, C. D. Murray, Eds. (Cambridge Univ. Press, 2018), pp. 338–362.
- M. R. Showalter, J. B. Pollack, M. E. Ockert, L. R. Doyle, J. B. Dalton, A photometric study of Saturn’s Ring. *Icarus* **100**, 394–411 (1992).
- M. R. Showalter, Disentangling Saturn’s F Ring. I. Clump orbits and lifetimes. *Icarus* **171**, 356–371 (2004).
- C. A. McGhee, P. D. Nicholson, R. G. French, K. J. Hall, HST observations of Saturnian Satellites during the 1995 ring plane crossings. *Icarus* **152**, 282–315 (2001).
- B. K. Meinke, L. W. Esposito, N. Albers, M. Sremčević, Classification of F ring features observed in Cassini UVIS occultations. *Icarus* **218**, 545–554 (2012).
- N. O. Attree, C. D. Murray, G. A. Williams, N. J. Cooper, A survey of low-velocity collisional features in Saturn’s F ring. *Icarus* **227**, 56–66 (2014).
- P. Goldreich, S. Tremaine, Towards a theory for the Uranian rings. *Nature* **277**, 97–99 (1979).
- M. R. Showalter, J. A. Burns, A numerical study of Saturn’s F-ring. *Icarus* **52**, 526–544 (1982).
- J. Scargle, J. Cuzzi, A. Dobrovolskis, L. Dones, R. Hogan, C. Levit, M. Showalter, K. Young, Dynamical evolution of Saturn’s rings in *AAS/Division for Planetary Sciences Meeting Abstracts* (Bulletin of the American Astronomical Society, 1993), vol. 25, p. 1103.
- O. C. Winter, D. C. Mourão, S. M. Giuliatti Winter, F. Spahn, C. da Cruz, Moonlets wandering on a leash-ring. *Mon. Not. R. Astron. Soc. Lett.*, L54–L57 (2007).
- O. C. Winter, D. C. Mourão, S. M. Giuliatti Winter, Short Lyapunov time: A method for identifying confined chaos. *Astron. Astrophys.* **523**, A67 (2010).
- S. M. Giuliatti Winter, D. C. Mourão, T. C. A. Freitas, The strands of the F ring disturbed by its closest satellites. *Adv. Space Res.* **38**, 781–787 (2006).
- N. J. Cooper, C. D. Murray, G. A. Williams, Local variability in the orbit of Saturn’s F Ring. *Astron. J.* **145**, 161 (2013).
- J. N. Cuzzi, A. D. Whizin, R. C. Hogan, A. R. Dobrovolskis, L. Dones, M. R. Showalter, J. E. Colwell, J. D. Scargle, Saturn’s F Ring core: Calm in the midst of chaos. *Icarus* **232**, 157–175 (2014).
- P. Goldreich, S. Tremaine, N. Borderies, Towards a theory for Neptune’s arc rings. *Astron. J.* **92**, 490 (1986).
- C. C. Porco, An explanation for Neptune’s ring arcs. *Science* **253**, 995–1001 (1991).
- J. N. Cuzzi, Corrigendum to Saturn’s F Ring core: Calm in the midst of chaos. *Icarus* **413**, 116011 (2024).
- E. A. Marouf, P. A. Rosen, Profiling Saturn’s rings by radio occultation. *Icarus* **68**, 120–166 (1986).
- J. E. Colwell, P. D. Nicholson, M. S. Tiscareno, C. D. Murray, R. G. French, E. A. Marouf, The Structure of Saturn’s Rings, in *Saturn from Cassini-Huygens*, M. Dougherty, L. W. Esposito, S. Krimigis, Eds. (Springer, 2009), p. 375.
- C. D. Murray, S. F. Dermott, *Solar System Dynamics* (Cambridge Univ. Press, 2012).
- R. G. French, C. A. McGhee, L. Dones, J. J. Lissauer, Saturn’s wayward shepherds: The peregrinations of Prometheus and Pandora. *Icarus* **162**, 143–170 (2003).
- P. Goldreich, N. Rappaport, Origin of chaos in the Prometheus-Pandora system. *Icarus* **166**, 320–327 (2003).
- J. N. Spitale, R. A. Jacobson, C. C. Porco, W. M. Owen Jr., The orbits of Saturn’s small satellites derived from combined historic and Cassini imaging observations. *Astron. J.* **132**, 692–710 (2006).
- J. N. Cuzzi, E. Marouf, R. French, R. Jacobson, F Ring Core Stability: Corotation Resonance Plus Antiresonance, in *AAS/Division for Planetary Sciences Meeting Abstracts* (American Astronomical Society, 2014), vol. 46, p. 402.01.
- E. Marouf, K. Wong, R. French, N. J. Rappaport, C. McGhee, Saturn’s F-Ring Discontinuous Core and Orbit Model, in *COSPAR Scientific Assembly* (COSPAR, 2010), vol. 38, p. 6.
- E. A. Marouf, K. Wong, R. French, N. Rappaport, C. McGhee, The Discontinuous Core of Saturn’s F-Ring and Orbit Model, in *AAS/Division for Planetary Sciences Meeting Abstracts* (Bulletin of the American Astronomical Society, 2010), vol. 42, p. 988.
- A. J. Kliore, J. D. Anderson, J. W. Armstrong, S. W. Asmar, C. L. Hamilton, N. J. Rappaport, H. D. Wahlquist, R. Ambrosini, F. M. Flasar, R. G. French, L. Iess, E. A. Marouf, A. F. Nagy, Cassini Radio Science. *Sp. Sci. Revs.* **115**, 1–70 (2004).
- F. S. Thomson, E. A. Marouf, G. L. Tyler, R. G. French, N. J. Rappaport, Periodic microstructure in Saturn’s rings A and B. *Geophys. Res. Lett.* **34**, 10.1029/2007GL032526 (2007).
- R. G. French, E. A. Marouf, N. J. Rappaport, C. A. McGhee, Occultation observations of Saturn’s B ring and Cassini division. *Astron. J.* **139**, 1649–1667 (2010).
- G. L. Tyler, E. A. Marouf, R. A. Simpson, H. A. Zebker, V. R. Eshleman, The microwave opacity of Saturn’s rings at wavelengths of 3.6 and 13 CM from Voyager 1 radio occultation. *Icarus* **54**, 160–188 (1983).
- A. S. Bosh, C. B. Olkin, R. G. French, P. D. Nicholson, Saturn’s F ring: Kinematics and particle sizes from stellar occultation studies. *Icarus* **157**, 57–75 (2002).
- N. Albers, M. Sremčević, J. E. Colwell, L. W. Esposito, Saturn’s F ring as seen by Cassini UVIS: Kinematics and statistics. *Icarus* **217**, 367–388 (2012).
- R. G. French, P. D. Nicholson, M. L. Cooke, J. L. Elliot, K. Matthews, O. Perkovic, E. Tollestrup, P. Harvey, N. J. Chanover, M. A. Clark, E. W. Dunham, W. Forrest, J. Harrington, J. Pipher, A. Brahic, I. Grenier, F. Roques, M. Arndt, Geometry of the Saturn system from the 3 July

- 1989 occultation of 28 SGR and Voyager observations. *Icarus* **103**, 163–214 (1993).
35. M. M. Hedman, P. D. Nicholson, K. H. Baines, B. J. Buratti, C. Sotin, R. N. Clark, R. H. Brown, R. G. French, E. A. Marouf, The architecture of the Cassini division. *Astron. J.* **139**, 228–251 (2010).
36. R. G. French, C. A. McGhee-French, K. Lonergan, T. Sepersky, R. A. Jacobson, P. D. Nicholson, M. M. Hedman, E. A. Marouf, J. E. Colwell, Noncircular features in Saturn's rings IV: Absolute radius scale and Saturn's pole direction. *Icarus* **290**, 14–45 (2017).
37. D. W. Foryta, B. Sicardy, The dynamics of the Neptunian ADAMS ring's arcs. *Icarus* **123**, 129–167 (1996).
38. F. Namouni, C. Porco, The confinement of Neptune's ring arcs by the moon Galatea. *Nature* **417**, 45–47 (2002).
39. M. Showalter, J. J. Lissauer, I. de Pater, R. S. French, A Three-Body Resonance Confines the Ring-Arcs of Neptune, in *AAS/Division for Planetary Sciences Meeting Abstracts* (American Astronomical Society, 2017), vol. 49, p. 104.01.
40. N. J. Cooper, S. Renner, C. D. Murray, M. W. Evans, Saturn's inner satellites: Orbits, masses, and the chaotic motion of Atlas from new *Cassini* Imaging observations. *Astron. J.* **149**, 27 (2015).
41. R. A. Jacobson, J. Spitale, C. C. Porco, K. Beurle, N. J. Cooper, M. W. Evans, C. D. Murray, Revised orbits of Saturn's small inner satellites. *Astron. J.* **135**, 261–263 (2008).
42. A. J. Farmer, P. Goldreich, Understanding the behavior of Prometheus and Pandora. *Icarus* **180**, 403–411 (2006).
43. S. Vahidinia, J. N. Cuzzi, M. Hedman, B. Draine, R. N. Clark, T. Roush, G. Filacchione, P. D. Nicholson, R. H. Brown, B. Buratti, C. Sotin, Saturn's F ring grains: Aggregates made of crystalline water ice. *Icarus* **215**, 682–694 (2011).
44. L. W. Esposito, B. K. Meinke, J. E. Colwell, P. D. Nicholson, M. M. Hedman, Moonlets and clumps in Saturn's F ring. *Icarus* **194**, 278–289 (2008).
45. R. S. French, M. R. Showalter, R. Sfair, C. A. Argüelles, M. Pajuelo, P. Becerra, M. M. Hedman, P. D. Nicholson, The brightening of Saturn's F ring. *Icarus* **219**, 181–193 (2012).
46. R. H. Durisen, N. L. Cramer, B. W. Murphy, J. N. Cuzzi, T. L. Mullikin, S. E. Cederbloom, Ballistic transport in planetary ring systems due to particle erosion mechanisms: I. Theory, numerical methods, and illustrative examples. *Icarus* **80**, 136–166 (1989).

Acknowledgments: We are very grateful to R. Jacobson for detailed, high-cadence orbital fits for Prometheus based on Cassini observations. We thank P. Nicholson and an anonymous reviewer for uncovering a fatal error in an earlier version; P. Goldreich and J. Scargle for valuable conversations; K. Wong for computational contributions; and D. Olson for graphics assistance. We also thank our reviewers of this version for their careful reading and useful suggestions for improvements. **Funding:** This work was supported by a Cassini Interdisciplinary Scientist grant to J.N.C. and Cassini RSS Team funding to E.A.M. and R.G.F.

Author contributions: J.N.C. conceived the hypothesis, performed the regressions, explained the discrepant data points, and wrote most of the paper. E.A.M. performed analysis of the RSS observations of the F ring used to generate the data reported in table S1, generated fig. S3, developed the Keplerian F ring core model reported in table S2, used the model to generate the detection and nondetection data reported in tables S3 and S4, and wrote the part of the Supplementary Materials relevant to the RSS observations. R.G.F. contributed F ring orbit and geometry calculations. C.D.M. contributed to the calculation of resonance locations and resonance variables, as well as the discussion of the structure and dynamics of the F ring environment. N.J.C. contributed to the discussion on dynamics, worked on the numerical computation of resonance locations and the resonance variable, and provided critical orbital information for Prometheus and the F ring. All authors contributed to proofreading, edits, and revisions. **Competing interests:** The authors declare that they have no competing interests.

Data and materials availability: All data needed to evaluate the conclusions in the paper are present in the paper and/or the Supplementary Materials. The complete set of raw Cassini RSS ring occultation data may be accessed from the Planetary Data System (PDS) Planetary Atmospheres Node (https://pds-atmospheres.nmsu.edu/data_and_services/atmospheres_data/catalog.htm#Saturn). A subset of RSS ring occultation profiles reconstructed to remove diffraction effects using data collected before the loss of the Cassini Ultra-Stable Oscillator (USO) in late 2011 may be accessed from the PDS Ring-Moon Systems Node (https://pds-rings.seti.org/viewmaster/volumes/CORSS_8xxx).

Submitted 30 October 2023

Accepted 8 April 2024

Published 10 May 2024

10.1126/sciadv.adl6601